COMMUNICATION

Cooperative enhancement of redox catalysis in divanadium complexes binucleated by 1,8-naphthyridine-2,7-dicarboxylate

Simran Simran,†[a] Maxym Tansky,†[b] Seth Trabulsi,[c] Liangzi Deng,[c] Ching-Wu Chu, [iD][c] Andrew Ozarowski [iD][d] and Robert J. Comito [iD] *[a]

We report discrete divanadium complexes of 1,8-naphthyridine-2,7-dicarboxylate, characterized by SCXRD, DFT modelling, and magnetometry. One complex shows significantly greater activity in the aerobic cleavage of diols and a lignin model compound than its monometallic analogs. Mechanistic experiments and a substrate-bound complex provide insight into cooperativity in vanadium redox catalysis.

Vanadium's earth abundance and nontoxicity make it an attractive alternative to precious metal catalysis,[1] especially in the oxidative cleavage of diols[2–5] and the depolymerization of lignin,[6–11] applications in which vanadium shows promising reactivity. However, vanadium suffers lower turnover and activity in these reactions than precious metals. This limitation has sometimes been attributed to inefficient two-electron redox cycling in vanadium,[12–14] which has a high reorganization energy and inefficient spin conversion. Redox cooperativity has been proposed to mitigate these limitations in vanadium catalysis by dividing two-electron redox steps into coupled one-electron steps, which have lower reorganization energies and spin barriers. This hypothesis has been best investigated in the aerobic oxidation of alcohols.[15–20] In some cases, higher catalytic activity was demonstrated with a divanadium complex compared with a monometallic analog.[18–22] However, few of the divanadium complexes in these studies have been binucleated in the sense that nuclearity was controlled by the ligand.[19,20] Instead, the vanadium centres are connected by labile µ-oxide or µ-alkoxide anions, introducing

some uncertainty into the aggregation and speciation during catalysis.

This study utilizes 1,8-naphthyridine-2,7-dicarboxylic acid (H_2ndc, **1**, Scheme 1) as a binucleating platform for carbohydrate upgrading, under the central hypothesis that redox cooperativity will deliver a more productive vanadium catalyst. Convenient for analysis of nuclearity, H_2ndc (**1**) has the close mononucleating analog 2,6-dipicolinic acid (H_2dipic) whose complexes VO(DMSO)$_2$(dipic) (**2**) and VO(OiPr)(dipic) (**3**) have already been studied as catalysts for alcohol oxidation,[23] oxidative diol cleavage,[2] and lignin depolymerization.[6,7,24] H_2ndc (**1**) also has precedent as a binucleating ligand in dinickel,[25] diruthenium,[26,27] and dirhodium[27] complexes.

Thus, metalation of H_2ndc (**1**) with two equivalents of VO(OiPr)$_3$ in DMSO or in pyridine (Py) gave us analogous complexes with the compositions V_2O_2(OiPr)$_2$(DMSO)$_2$(ndc)·DMSO (**4**) and V_2O_2(OiPr)$_2$(Py)$_2$(ndc) (**5**, Scheme 1A). NMR analysis of the supernatant showed that three equivalents of isopropanol and one equivalent of acetone are also formed, which explains the apparent reduction of V^V to V^{IV} (section S4.2, Fig. S13). Single-crystal X-ray diffraction (SCXRD) analysis of **4** and of **5** both resulted in a binucleated divanadium structure, with two vanadyl units bridged both by the ndc^{2-} ligand and by two µ-isopropoxides (Scheme 1A). The two complexes are roughly C_2 symmetric, with both vanadium centres having similar six-coordinate and pseudo-octahedral primary coordination spheres completed by oxido and solvent coordination. The bond lengths in **4** are very similar to those reported for VO(DMSO)$_2$(dipic) (**2**, see Table S8 for comparison). Bond valence sum analysis of **4** and of **5** resulted in values of 3.843–3.925 (sections S5.2 and 6), supporting our V^{IV,IV} oxidation state assignment. The two vanadyl centres are nearly coplanar but not parallel, with an O–V–V–O dihedral angle of 1.6° and O–V–V angles of 114.9° and 114.0° in **4**. The divanadyl unit is also twisted relative to the naphthyridine ring, with a V–N–N–V dihedral angle of 27.2° in **4**.
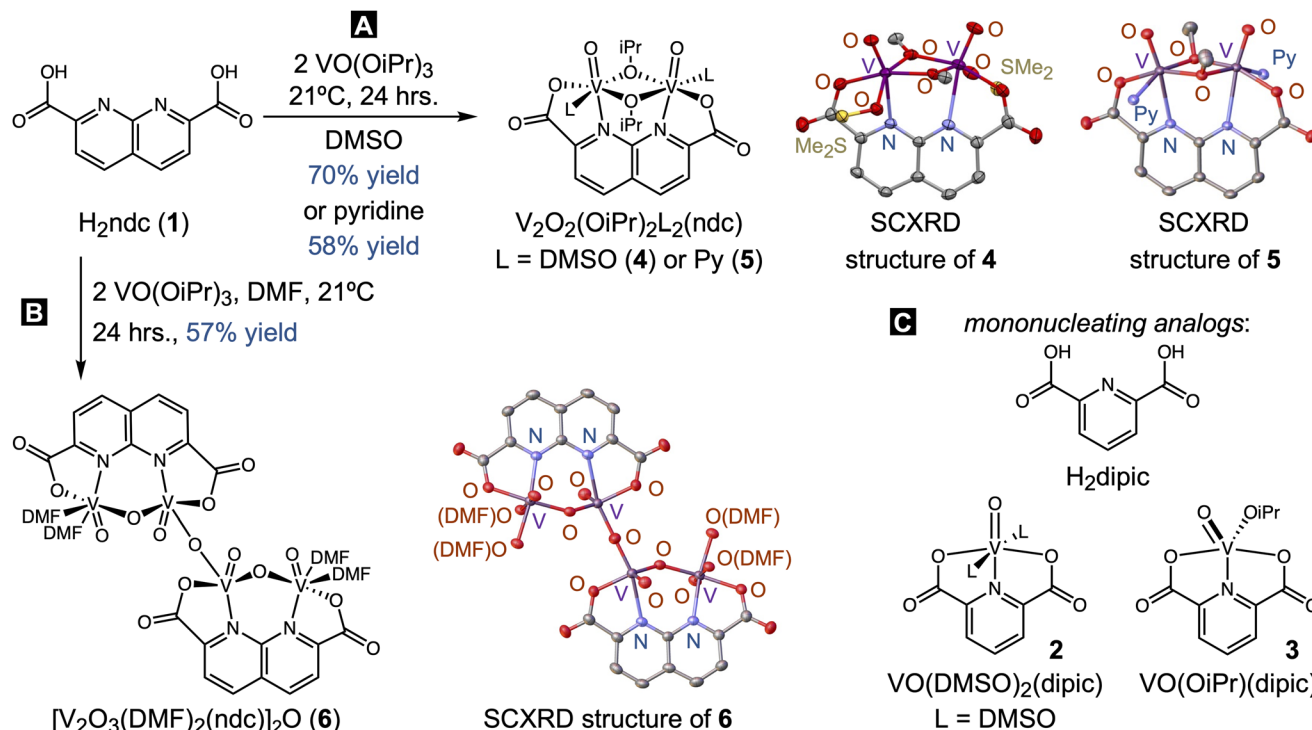
[a]Department of Chemistry, University of Houston, Houston, Texas, 77204, USA
[b]Department of Chemistry and Biotechnology, Graduate School of Engineering, The University of Tokyo, Tokyo 113-8656, Japan. E-mail: rjcomito@central.uh.edu
[c]Department of Physics, Texas Center for Superconductivity, University of Houston, 3369 Cullen Blvd, Houston, TX, 77204-5002, USA
[d]National High Magnetic Field Laboratory, 1800 E. Paul Dirac Dr, Tallahassee, Fl, 32310-3706, USA
† These authors contributed equally.

Scheme 1 Synthesis of complexes **4**, **5**, and **6** with their SCXRD structures and mononucleating analogs. Thermal ellipsoids are 50% equiprobability envelopes. Hydrogens, methyl groups, and additional solvent molecules were removed for clarity.

In contrast to DMSO and pyridine, metalation in DMF gave a tetravanadium complex with the composition $[V_2O_3(DMF)_2(ndc)]_2O \cdot DMF$ (**6**), consisting of two binucleated divanadium centres bridged by a μ-oxide as characterized by SCXRD (Scheme 1B). Complex **6** shows distinct five- and six-coordinate vanadium sites, with bond valence sums of 4.339 and 4.072 respectively (section S5.4, Table S16). Together, with a formula that indicates an average vanadium oxidation state of 4.5, **6** likely exhibits $V^{V,IV}$ mixed valence.[28]

Then, we performed geometry optimizations of $V_2O_2(OiPr)_2(DMSO)_2(ndc)$ (**4**), finding the triplet (**S7-DFT**-triplet) to be lower in free energy by 2.57 kcal mol^{-1} than the singlet (**S7-DFT**-singlet, PBE/6-311G(2d,p), section S7.1). Mulliken spin density analysis of **S7-DFT**-triplet resulted in values of +1.031 and +1.037 on the two vanadium atoms, confirming our assignment of two d^1 V^{IV} centres.

Consistently, magnetometry analysis indicated moderate ferromagnetism in $V_2O_2(OiPr)_2(DMSO)_2(ndc) \cdot DMSO$ (**4**), as evidenced by a strong increase in molar magnetic susceptibility (χ_M) at low temperatures with no local maximum (Fig. 1A). Similarly, $\chi_M T$ exhibits a maximum of 0.85 emu K mol^{-1} Oe^{-1} at 11 K with a sudden decrease below 10 K caused by the Zeeman splitting, characteristic of a high-spin ground state. Fitting of the $\chi_M T$ curve gave the exchange integral $J =$ -31 cm^{-1} based on the Heisenberg–Dirac–van Vleck Hamiltonian $\mathcal{H} = J\hat{S}_1\hat{S}_2$, where $\hat{S}_1$ and $\hat{S}_2$ are the spin operators of the interacting ions, and the coupling constant J represents the singlet–triplet energy gap. In this notation, the exchange interaction is ferromagnetic for $J < 0$. A low but not unprecedented g factor of 1.88 was also derived from the fit.[29] The peak value of $\chi_M T = 0.85$ emu K mol^{-1} Oe^{-1} approaches the theoretical maximum value of 0.88, calculated for spin 1 with for $g = 1.88$. Together, these data indicate a moderate ferromagnetic interaction with nearly full population of the triplet state at low temperature. The coupling interaction between vanadyl centers in **1** was also probed by broken symmetry magnetic coupling analysis (B3LYP-G/def2/J-TZVPP, section S7.2) performed using the geometry-optimized structure of **1**. The resulting J value of -27 cm^{-1} further confirms the ferromagnetic assignment. Finally, the overlap integral reported by ORCA for the two vanadyl d_{xy} orbitals is very low (0.028), thus favoring the ferromagnetic interaction. Indeed, the two singly-occupied molecular orbitals (SOMOs) in **S7-DFT**-triplet (Fig. S23 and S24) differ in energy by 3.46 kcal mol^{-1}, and are predominantly the in-phase and out-of-phase combinations of the two vanadyl d_{xy} orbitals, with secondary contributions by the carboxylate and the μ-oxygen atom.

This ferromagnetism is unexpected for a $V^{IV,IV}$ complex with a $[VO(\mu\text{-}OR)_2VO]^{2+}$ core in this geometry. Plass developed a geometric classification for magnetically coupled metal centres,[30] under which $V_2O_2(OiPr)_2(DMSO)_2(ndc) \cdot DMSO$ (**4**) counts as *syn*-orthogonal. Direct exchange between the d_{xy} orbitals is expected to lead to strong antiferromagnetism by d^1 centers in a *syn*-orthogonal geometry.[31] Consistently, all reported *syn*-orthogonal divanadyl complexes are antiferromagnetically coupled,[32–37] although ferromagnetism has been
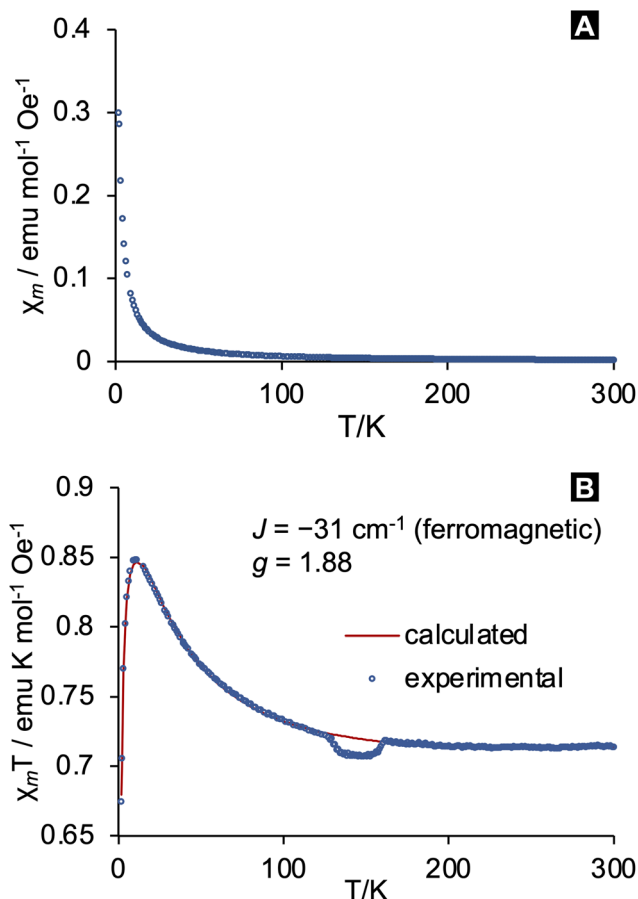
Fig. 1 (A) Molar magnetic susceptibility χ_M for complex **4**. (B) $\chi_M T$ as a function of temperature. All measurements were done at 2 T using powdered sample.

reported for divanadyls in an *anti*-orthogonal[38] and other geometries. Presumably, lack of coplanarity (40.4°) between the two d_{xy} orbitals in **4** mitigates direct exchange, a consequence of the nonparallel arrangement of the two vanadyl units. Indeed, the O≡V–V angles in **4** (114.9°, 114.0°) are significantly greater than those of the published antiferromagnetic compounds, although the V–V distance in **4** (3.105 Å) is similar those of the published compounds (see comparison in Table S42). Distortions from Plass's idealized geometries are known to significantly reduce antiferromagnetic coupling.[39] One explanation for the ferromagnetism of **4** is superexchange through the μ-alkoxides. Along these lines, the lower energy SOMO2 depicts extensive delocalization between vanadyl centres through the bridging alkoxide oxygen atoms (Fig. S24).

We initiated our catalytic studies by comparing vanadium catalysts at low loading (2 mol% V) in the aerobic cleavage of pinacol (**7**) at 50 °C for 24 hours (Table 1). Complex $V_2O_2(OiPr)_2(DMSO)_2(ndc)\cdot DMSO$ (**4**) showed the highest conversion and yield of acetone (**10**, 37%), compared with multimetallic complexes **5** and **6**, monometallic analogs **2** and **3**, and simple vanadium precursors (entries 1–8). For this reason and because of its homology to **2**, we focused the rest of our

catalytic and analytical studies on complex **4**. At 72 hours, **4** gave 79% yield of **10** (entry 9). **4** also gave good yields in the aerobic cleavage of diols **8** and **9** at 24 hours (entries 12 and 15). Monovanadium dipic^{2-} complexes **2** and **3** underperformed bimetallic complex **4** significantly in the cleavage of **7** and **9**, and modestly in the cleavage of **8**, supporting our hypothesis of cooperativity. Catalyst omission results in 0% conversion of **7**, 15% conversion of **8**, and 0% conversion of **9** (Table S6.1, entries 12, 16, and 20).

Cyclic voltammetry comparison of vanadium(IV) complexes $V_2O_2(OiPr)_2(DMSO)_2(ndc)\cdot DMSO$ (**4**) and $VO(DMSO)_2(dipic)$ (**2**) does not show clear evidence for outer-sphere redox cooperativity but instead similar first reduction and first oxidation features. Scanning from 0.00 to +1.50 resulted in irreversible oxidations at $E_{p,a}$ = +1.26 V for **4** and +1.29 V for **2** (*vs.* Ag/AgClO$_4$, section S8, Fig. S30), presumably the V^{IV}/V^V couple. Reductive scans (0.00 to −0.80 V) gave an irreversible reduction at $E_{p,c}$ = −0.58 V for **4** and a quasireversible reduction at $E_{p,c}$ = −0.66 V for **2** (Fig. S33), presumably the V^{IV}/V^{III} couple. There are no additional features suggesting partial oxidation or reduction of **4** to mixed-valent V^{IV,V} or V^{III,IV} states.

Nevertheless, the isolation of vanadium-bridging substrate-bound complexes does suggest cooperative substrate activation. Anaerobic reaction between pinacol (**7**) and $V_2O_2(OiPr)_2(DMSO)_2(ndc)\cdot DMSO$ (**4**) in pyridine at 50 °C did not give significant yields of acetone (section S6.2), but instead gave substrate adduct $V_2O_2(HPin)_2(ndc)\cdot 2Py$ (**14**, H$_2$Pin = **7**, Scheme 2). We also obtained an analogous complex with the composition $V_2O_2(HPin)_2(ndc)$ (**15**) by the reaction of **4** and **7** in DMF at 100 °C. The SCXRD structures of **14** and **15** are analogous to those for **4** and **5**, the HPin$^-$ unit replacing the μ-alkoxide and the coordinating solvent. They differ from each other only in the hydrogen-bonding of pyridine to the O–H bond in **14**. The apparent thermal stability of **14** and **15** contrasts with reported reactivity of monometallic analog VO(HPin)(dipic) (**16**),[2] which at 25 °C in pyridine readily gives acetone, pinacol (**7**), and a reduced complex VO(Py)$_2$(dipic). However, VO(Hpin)(dipic) (**16**) is V^V and thus more prone to reductive cleavage than the apparently V^{IV,IV} complexes **14** and **15**. On this basis, we propose a mechanism in which a V^{IV,IV} complex first coordinates the diol, then is oxidized by O$_2$ to a V^{V,V} complex, and finally cleaves the diolate regenerating a V^{IV,IV} complex.

Cooperativity could enhance any of these steps. However, given that monovanadium dipic^{2-} complexes undergo diol coordination and reductive fragmentation at room temperature, we argue that the oxidation with O$_2$ must benefit the most from redox cooperativity. Future mechanistic investigation in this laboratory will focus on the reactions between our V^{IV,IV} complexes and O$_2$. Unfortunately, we did not isolate **14** or **15** in sufficient bulk purity to evaluate their reactivity.

We next studied the aerobic cleavage of lignin model **17** (Table 1). Comparing polar solvents DMSO, pyridine, and DMF at 100 °C with low loading (1 mol% **4**, entries 18–20), we found that DMF gave the highest conversion of **17** (98%) and the

Table 1 Aerobic cleavage of diols and a lignin model compound

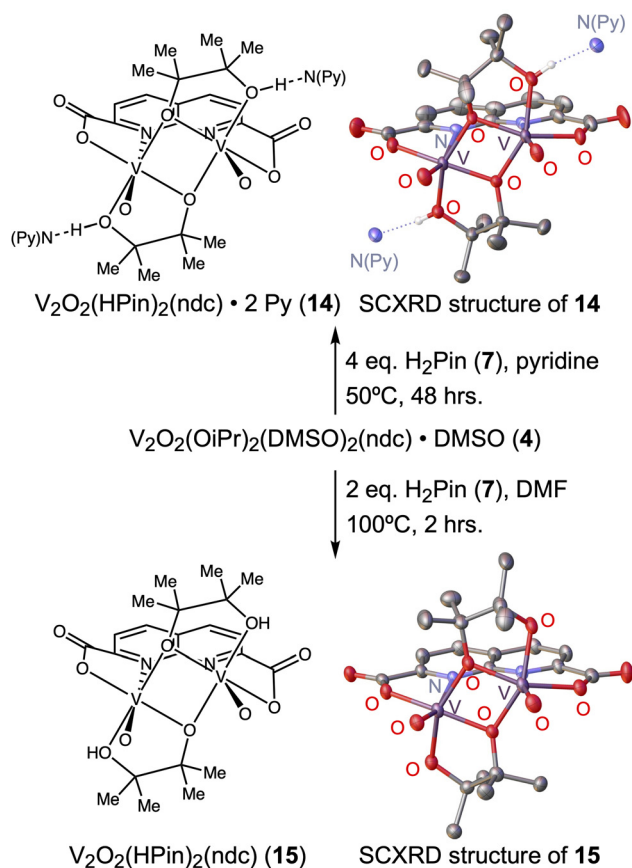| Entry	Catalyst (loading)	Reaction time	Solvent	T (°C)	Conversion, (substrate)[a]	Yield (product)[a]
1	V$_2$O$_2$(OiPr)$_2$(DMSO)$_2$(ndc)·DMSO (**4**, 1 mol%)	24 h	Pyridine	50	37% **7**	37% **10**
2	V$_2$O$_2$(OiPr)$_2$(Py)$_2$(ndc) (**5**, 1 mol%)	24 h	Pyridine	50	17% **7**	11% **10**
3	[V$_2$O$_3$(DMF)$_2$(ndc)]$_2$O·DMF (**6**, 1 mol%)	24 h	Pyridine	50	12% **7**	18% **10**
4	VO(DMSO)$_2$(dipic) (**2**, 2 mol%)	24 h	Pyridine	50	0% **7**	0% **10**
5	VO(OiPr)(dipic) (**3**, 2 mol%)	24 h	Pyridine	50	2% **7**	2% **10**
6	VO(OiPr)$_3$ (2 mol%)	24 h	Pyridine	50	5% **7**	4% **10**
7	VO(SO$_4$) (2 mol%)	24 h	Pyridine	50	1% **7**	1% **10**
8	V$_2$O$_5$ (1 mol%)	24 h	Pyridine	50	4% **7**	4% **10**
9	V$_2$O$_2$(OiPr)$_2$(DMSO)$_2$(ndc)·DMSO (**4**, 1 mol%)	72 h	Pyridine	50	84% **7**	79% **10**
10	VO(DMSO)$_2$(dipic) (**2**, 2 mol%)	72 h	Pyridine	50	3% **7**	3% **10**
11	VO(OiPr)(dipic) (**3**, 2 mol%)	72 h	Pyridine	50	5% **7**	5% **10**
12	V$_2$O$_2$(OiPr)$_2$(DMSO)$_2$(ndc)·DMSO (**4**, 1 mol%)	24 h	Pyridine	50	68% **8**	54% **11**
13	VO(DMSO)$_2$(dipic) (**2**, 2 mol%)	24 h	Pyridine	50	55% **8**	42% **11**
14	VO(OiPr)(dipic) (**3**, 2 mol%)	24 h	Pyridine	50	55% **8**	48% **11**
15	V$_2$O$_2$(OiPr)$_2$(DMSO)$_2$(ndc)·DMSO (**4**, 1 mol%)	24 h	Pyridine	50	99% **9**	88% **12**, 7% **13**
16	VO(DMSO)$_2$(dipic) (**2**, 2 mol%)	24 h	Pyridine	50	15% **9**	14% **12**, 1% **13**
17	VO(OiPr)(dipic) (**3**, 2 mol%)	24 h	Pyridine	50	25% **9**	22% **12**, 2% **13**
18	V$_2$O$_2$(OiPr)$_2$(DMSO)$_2$(ndc)·DMSO (**4**, 1 mol%)	48 h.	DMSO	100	44% **17**	3% **13**, 3% **18**, 2% **12**, 30% **19**
19	V$_2$O$_2$(OiPr)$_2$(DMSO)$_2$(ndc)·DMSO (**4**, 1 mol%)	48 h	Pyridine	100	74% **17**	24% **13**, 10% **18**, 2% **12**, 25% **19**
20	V$_2$O$_2$(OiPr)$_2$(DMSO)$_2$(ndc)·DMSO (**4**, 1 mol%)	48 h	DMF	100	98% **17**	85% **13**, 72% **18**, 5% **12**, 2% **19**
21	V$_2$O$_2$(OiPr)$_2$(DMSO)$_2$(ndc)·DMSO (**4**, 1 mol%)	48 h	DMF	22	1% **17**	0% **13**, <1% **18**, 0% **12**, <1% **19**
22	V$_2$O$_2$(OiPr)$_2$(DMSO)$_2$(ndc)·DMSO (**4**, 1 mol%)	48 h	DMF	60	50% **17**	13% **13**, 15% **18**, 1% **12**, 26% **19**
23	V$_2$O$_2$(OiPr)$_2$(DMSO)$_2$(ndc)·DMSO (**4**, 1 mol%)	48 h	DMF	80	92% **17**	26% **13**, 49% **18**, 4% **12**, 26% **19**
24	V$_2$O$_2$(OiPr)$_2$(DMSO)$_2$(ndc)·DMSO (**4**, 1 mol%)	48 h	DMF	120	>99% **17**	44% **13**, 74% **18**, 5% **12**, <1% **19**
25	V$_2$O$_2$(OiPr)$_2$(DMSO)$_2$(ndc)·DMSO (**4**, 0.5 mol%)	48 h	DMF	100	90% **17**	50% **13**, 55% **18**, 8% **12**, 7% **19**
26	V$_2$O$_2$(OiPr)$_2$(DMSO)$_2$(ndc)·DMSO (**4**, 2 mol%)	48 h	DMF	100	>99% **17**	85% **13**, 75% **18**, 3% **12**, 1% **19**
27	V$_2$O$_2$(OiPr)$_2$(DMSO)$_2$(ndc)·DMSO (**4**, 5 mol%)	48 h	DMF	100	>99% **17**	82% **13**, 99% **18**, 2% **12**, <1% **19**
28	VO(DMSO)$_2$(dipic) (**2**, 2 mol%)	48 h	DMF	100	31% **17**	7% **13**, 9% **18**, 3% **12**, 6% **19**
29	VO(OiPr)(dipic) (**3**, 2 mol%)	48 h	DMF	100	24% **17**	6% **13**, 6% **18**, 3% **12**, 7% **19**

[a] Substrate conversion and product yields determined by crude ^{1}H NMR with an internal standard.

highest yields of cleavage products **13** and **18** (85% and 72%). DMSO and pyridine gave the major product **19**, which we confirmed was an intermediate in the oxidation of **17** (section S6.5). Then, we screened temperatures in DMF (entries 20–24), obtaining higher yields of **13** at 100 °C than at 22 °C, 60 °C, 80 °C, or 120 °C. 1 mol% loading of **4** proved optimal, as lower loading resulted in lower yields while higher loadings did not show significant increases in yields (entries 25–27). Finally, monometallic analogs VO(DMSO)$_2$(dipic) (**2**) and VO(OiPr)(dipic) (**3**) significantly underperformed divanadium **4** under analogous conditions with a fixed loading of 2 mol% vanadium (entries 28 and 29), further supporting our claim of bimetallic cooperativity. Simple vanadium sources VO(OiPr)$_3$,

VO(SO$_4$), and V$_2$O$_5$ are also poor catalysts under these conditions (section S6.3).

In summary, complex V$_2$O$_2$(OiPr)$_2$(DMSO)$_2$(ndc)·DMSO (**4**) outperforms its monometallic analogs in the aerobic cleavage of diols and of lignin model **17**. Its maximum turnover number (90) exceeds those reported for vanadium-catalysed diol[2–5] or lignin cleavage[6–11] (Table S40). These results validate the hypothesis that cooperativity enhances the productivity of vanadium redox catalysis. They also provide a binucleating platform for studying redox cooperativity and for catalyst optimization with vanadium and other base metals. Finally, this report will inform the quest for sustainable catalysts for the upgrading of carbohydrates and biomass.

Scheme 2 Isolation of substrate-bound complexes 14 and 15. Thermal ellipsoids are 50% equiprobability envelopes. Hydrogens and additional solvent molecules were removed for clarity.

ation data, spectra, catalytic tables, magnetometry data, computational data, crystallographic data, and cyclic voltammetry data. See DOI: https://doi.org/10.1039/d5dt01296a.

CCDC 2382161, 2446197–2446199 and 2446206 contain the supplementary crystallographic data for this paper.[40a–e]

Acknowledgements

Author contributions

Simran Simran: investigation, methodology, writing – review & editing. Maxym Tansky: investigation, validation, writing – original draft, review & editing. These authors contributed equally. Seth Trabulsi: investigation. Liangzi Deng: investigation, methodology, writing – review & editing. Ching-Wu Chu: resources, supervision. Andrew Ozarowski: investigation, methodology, visualization, writing – original draft, review & editing. Robert J. Comito: conceptualization, funding acquisition, methodology, project administration, resources, supervision, visualization, writing – original draft, review & editing.

Conflicts of interest

There are no conflicts to declare.

Data availability

The data supporting this article have been included as a part of supplementary information (SI). The Supplementary Information file contains synthetic procedures, characteriz-

References

1 R. R. Langeslay, D. M. Kaphan, C. L. Marshall, P. C. Stair, A. P. Sattelberger and M. Delferro, *Chem. Rev.*, 2019, **119**, 2128.

2 S. K. Hanson, R. T. Baker, J. C. Gordon, B. L. Scott, A. D. Sutton and D. L. Thorn, *J. Am. Chem. Soc.*, 2009, **131**, 428.

3 M. Kirihara, K. Yoshida, T. Noguchi, S. Naito, N. Matsumoto, Y. Ema, M. Torii, Y. Ishizuki and I. Souta, *Tetrahedron Lett.*, 2010, **51**, 3619.

4 W. Wang, M. Niu, Y. Hou, Z. Liu, Q. Liu, S. Ren and K. N. Marsh, *Green Chem.*, 2014, **16**, 2614.

5 Z. Tang, W. Deng, Y. Wang, E. Zhu, X. Wan, Q. Zhang and Y. Wang, *ChemSusChem*, 2014, **7**, 1557.

6 S. K. Hanson and R. T. Baker, *Acc. Chem. Res.*, 2015, **48**, 2037.

7 S. K. Hanson, R. Wu and L. A. P. Silks, *Angew. Chem., Int. Ed.*, 2012, **51**, 3410.

8 H. J. Parker, C. J. Chuch, T. Woodman and M. D. Jones, *Catal. Today*, 2016, **269**, 40.

9 F. Walch, O. Y. Abdelaziz, S. Meier, S. Bjelic, C. P. Hulteberg and A. Riisager, *Catal. Sci. Technol.*, 2021, **11**, 1843.

10 J. M. W. Chan, S. Bauer, H. Sorek, S. Sreekumar, K. Wang and F. D. Toste, *ACS Catal.*, 2013, **3**, 1369.

11 G. F. D. De Gregorio, R. Prado, C. Vriamont, X. Erdocia, J. Labidi, J. P. Hallett and T. Welton, *ACS Sustainable Chem. Eng.*, 2016, **4**, 6031.

12 Y.-Y. Jiang, L. Yan, H.-Z. Yu, Q. Zhang and Y. Fu, *ACS Catal.*, 2016, **6**, 4399.

13 L. C. De Vicente Poutás, M. C. Reis, R. Sanz, C. S. López and O. N. Faza, *Inorg. Chem.*, 2016, **55**, 11372.

14 Y.-Y. Jiang, J.-L. Jiang and Y. Fu, *Organometallics*, 2016, **35**, 3388.

15 X. Fan, J. Ma, M. Wang, M. Gao and J. Xu, *ACS Catal.*, 2024, **14**, 10538.

16 J. K. Elinburg, S. L. Carter, J. J. M. Nelson, D. G. Fraser, M. P. Crockett, A. B. Beeler, E. Nordlander, A. L. Rheingold and L. H. Doerrer, *Inorg. Chem.*, 2020, **59**, 16500.

17 M. I. Kitt, E. Amir, E. R. Sloane, D. G. Fraser, J. E. Cerritelli, C. S. M. Sabanos, J. H. McNeely, J. K. Snyder, L. H. Doerrer and A. B. Beeler, *ACS Catal.*, 2024, **14**, 4799.

18 E. Hoppe and C. Limberg, *Chem. – Eur. J.*, 2007, **13**, 7006.

19 E. Hoppe, C. Limberg and B. Ziemer, *Inorg. Chem.*, 2006, **45**, 8308.

20 C. Limberg, *Eur. J. Inorg. Chem.*, 2007, **2007**, 3303.

21 C. G. Werncke, C. Limberg and R. Metzinger, *Z. Anorg. Allg. Chem.*, 2013, **639**, 2426.

22 C. G. Werncke, C. Limberg, C. Knispel and S. Mebs, *Chem. – Eur. J.*, 2011, **2011**, 12129.

23 S. K. Hanson, R. T. Baker, J. C. Gordon, B. L. Scott, L. A. Silks and D. L. Thorn, *J. Am. Chem. Soc.*, 2010, **132**, 17804.

24 S. K. Hanson, R. T. Baker, J. S. Gordon, B. L. Scott and D. L. Thorn, *Inorg. Chem.*, 2010, **49**, 5611.

25 H. Aghabozorg, R. C. Palenik and G. J. Palenik, *Inorg. Chem.*, 1985, **24**, 4214.

26 C.-H. Lee, C.-L. Wu, S.-A. Hua, Y.-H. Liu, S.-M. Peng and S.-T. Liu, *Eur. J. Inorg. Chem.*, 2015, **2015**, 1417.

27 J.-P. Collin, A. Jouaiti, J.-P. Sauvage, W. C. Kaska, M. A. McLoughlin, N. L. Keder, W. T. A. Harrison and G. D. Stucky, *Inorg. Chem.*, 1990, **29**, 2238.

28 S. Nitsche, S. Schmitz, K. Stirnat, A. Sandleben and A. Klein, *Z. Anorg. Allg. Chem.*, 2018, **644**, 1805.

29 N. S. Dean, M. R. Bond, C. J. O'Connor and C. J. Carrano, *Inorg. Chem.*, 1996, **35**, 7643.

30 W. Plass, *Angew. Chem., Int. Ed. Engl.*, 1996, **35**, 627.

31 A. P. Ginsberg, E. Koubek and H. J. Williams, *Inorg. Chem.*, 1966, **5**, 1656.

32 A. Rodríguez-Fortea, P. Alemany, S. Alvarez and E. Ruiz, *Eur. J. Inorg. Chem.*, 2004, **2004**, 143.

33 A. Ozarowski and D. Reinen, *Inorg. Chem.*, 1986, **25**, 1704.

34 C. J. Carrano, C. M. Nunn, R. Quan, J. A. Bonadies and V. L. Pecoraro, *Inorg. Chem.*, 1990, **29**, 944.

35 S. L. Castro, M. E. Cass, F. J. Hollander and S. L. Bartley, *Inorg. Chem.*, 1995, **34**, 466.

36 Y. Sun, M. Melchior, D. A. Summers, R. C. Thompson, S. J. Rettig and C. Orvig, *Inorg. Chem.*, 1998, **37**, 3119.

37 A. Neves, K. Wieghardt, B. Nuber and J. Weiss, *Inorg. Chim. Acta*, 1988, **150**, 183.

38 Z. Janas, J. Jezierska, A. Ozarowski, A. Bienko, T. Lis, A. Jezierski and M. Krawczyk, *Dalton Trans.*, 2021, **50**, 5184.

39 A. S. Ceccato, A. Neves, M. A. de Brito, S. M. Dreschel, A. S. Mangrich, R. Werner, W. Haase and A. J. Bortoluzzi, *J. Chem. Soc., Dalton Trans.*, 2000, 1573.

40 (*a*) CCDC 2382161: Experimental Crystal Structure Determination, 2025, DOI: **10.5517/ccdc.csd.cc2kytx8**; (*b*) CCDC 2446197: Experimental Crystal Structure Determination, 2025, DOI: **10.5517/ccdc.csd.cc2n3glv**; (*c*) CCDC 2446198: Experimental Crystal Structure Determination, 2025, DOI: **10.5517/ccdc.csd.cc2n3gmw**; (*d*) CCDC 2446199: Experimental Crystal Structure Determination, 2025, DOI: **10.5517/ccdc.csd.cc2n3gnx**; (*e*) CCDC 2446206: Experimental Crystal Structure Determination, 2025, DOI: **10.5517/ccdc.csd.cc2n3gw4**.